Origins of Negative Gas Adsorption

Jack Evans, Lyderic Bocquet, François-Xavier Coudert

Origins of Negative Gas Adsorption

Jack D. Evans[a], Lydéric Bocquet[b], François-Xavier Coudert[a]

[a] *Chimie ParisTech, PSL Research University, CNRS, Institut de Recherche de Chimie Paris, 75005 Paris, France*
[b] *Laboratoire de Physique Statistique, École Normale Supérieure, UMR CNRS 8550, PSL Research University, 24 rue Lhomond, 75005 Paris, France*

SUMMARY

Negative gas adsorption by a porous crystalline solid, DUT-49, observed by spontaneous desorption of gas during a pressure increase, raises fundamental questions on the physical origin of this puzzling behavior. Importantly, a framework able to transform a large amount of strain into pressure has many possible technological applications. To address this question, we have performed a combined study of the mechanics and thermodynamics of DUT-49 at both the molecular unit and framework scales, employing quantum density functional theory and extensive classic molecular dynamics simulations. We demonstrate that negative gas adsorption takes its origin from a molecular buckling of the organic structural unit, allowing a colossal framework transformation. Methane adsorption is subsequently shown to activate this transition, in full agreement with experimental observations. The molecular insight, presented here, has unveiled the mechanics and thermodynamics responsible for negative gas adsorption and provides unparalleled understanding to aid the discovery of new examples of similarly responsive porous metamaterials.

Keywords: nanoporous materials, thermodynamics, mechanics, gas adsorption, methane, stimuli-responsive

The Bigger Picture

Conventional nanoporous materials have a wide range of technological applications as desiccants, ion exchangers and catalysts. However, it is increasingly evident that emerging flexible metal–organic framework materials are particularly advantageous in separation processes and responsive applications. In particular, the flexible material DUT-49 shows an unexpected

phenomenon where, as the material fills with gas, it contracts suddenly and releases a significant portion of methane. This negative gas adsorption process is extremely rare and has not been observed in porous materials previously. Here, we demonstrate the mechanics and thermodynamics responsible for this non-conventional behavior using multi-scale computer simulations. This fundamental understanding is crucial for the application of negative gas adsorption materials, such as advanced micro-pneumatic components and stimuli-responsive separation processes.

Introduction

Metal–organic frameworks (MOFs) differ from conventional inorganic porous materials in that many demonstrate large-scale flexibility of their structure, which results in appealing physical and chemical properties.[1] Notably, there are increasing reports of these soft porous crystals[2] whose flexibility manifests by large-scale transformations induced by modest physico-chemical stimulation, such as changes in temperature, mechanical constraints, and guest adsorption.[3] Among the large variety of behavior exhibited by stimuli-responsive materials, we can cite the widely studied phenomena of gated adsorption and breathing,[4] which have applications in gas separations,[5] storage[6] and sensing.[7]

A particularly intriguing phenomenon resulting from this soft nature of metal–organic frameworks (MOFs) is that of negative gas adsorption (NGA) in DUT-49, which was recently reported by Kaskel and coworkers.[8] DUT-49 is a MOF constructed from dinuclear paddlewheel copper(II) metal centers and 9,9′-([1,1′-biphenyl]-4,4′-diyl)bis(9H-carbazole-3,6-dicarboxylate (BBCDC) linkers, forming a cubic mesoporous framework displayed in Figure 1a.[9] Laws of thermodynamics mandate that, at equilibrium and at constant temperature, the absolute amount of substance in the adsorbed phase increases with increasing pressure of the adsorbate, which results in the positive slopes observed for single-component adsorption isotherms.[10] However, upon adsorption of gases such as methane or *n*-butane, DUT-49 displays a NGA step depicted in Figure 1b, causing an unexpected pressure amplification triggered by a sudden structural transition of the nanoporous framework. It is the first material known to exhibit this property, which was attributed to the filling of the micropores by guests and the occurrence of a metastable state of the loaded framework. However, there has been so far

no direct account of the microscopic nature of the transition itself, and the detailed balance of thermodynamic driving forces is unknown.

In situ X-ray diffraction was used to elucidate the open pore (*op*) and contracted pore (*cp*) structures of DUT-49 as depicted in Figure 1a. The structural transformation observed in this material — linked to the NGA — is localized to a deformation of the BBCDC ligand, Figure 1c. This is in stark contrast with previously known examples of large structural transitions in MOFs, where organic linkers are seen as rigid struts. Commonly, flexible MOFs rely upon either a hinging mechanism, where the deformation occurs in the coordination of the metal node,[11, 12, 13] or sub-lattice displacement[14] as stylistically illustrated in Figure 1d. Moreover the periodic array of geometrically and elastically coupled buckling units in DUT-49 is analogous to the folding and unfolding of maps, wings, petals and the artificially constructed Miura-ori pattern.[15, 16] We thus hypothesize the deformation observed for the ligand, and the collective behavior coupling these deformations throughout the crystal, is crucial to the NGA phenomenon allowing for an accessible, rapid, and large structural transformation.

Herein, we detail multiscale molecular simulations of DUT-49 to provide insight into the mechanics and thermodynamics of the NGA transition, linking this astonishing macroscopic behavior to a mechanism at the atomistic scale. We combine quantum chemistry calculations at the density functional theory (DFT) level with classical molecular dynamics simulations to provide a complete picture of this phenomenon.

Results and Discussion

To provide understanding at the microscopic level of the negative gas adsorption transition, we combined a variety of methods including DFT calculations of the vital components of the DUT-49 framework and classical simulation of the crystal and adsorbates.

Ligand mechanics

Initial investigation of the experimental crystal structures of DUT-49, *op* and *cp*, shows that the copper paddlewheel environment is almost undeformed in the *cp* structure, while the BBCDC ligand is significantly bent — with the deformation localized on the biphenyl unit. This behavior of the ligand is akin, in the world of macroscopic mechanics, to the buckling of a column upon the application of a critical load.[17] The phenomena of

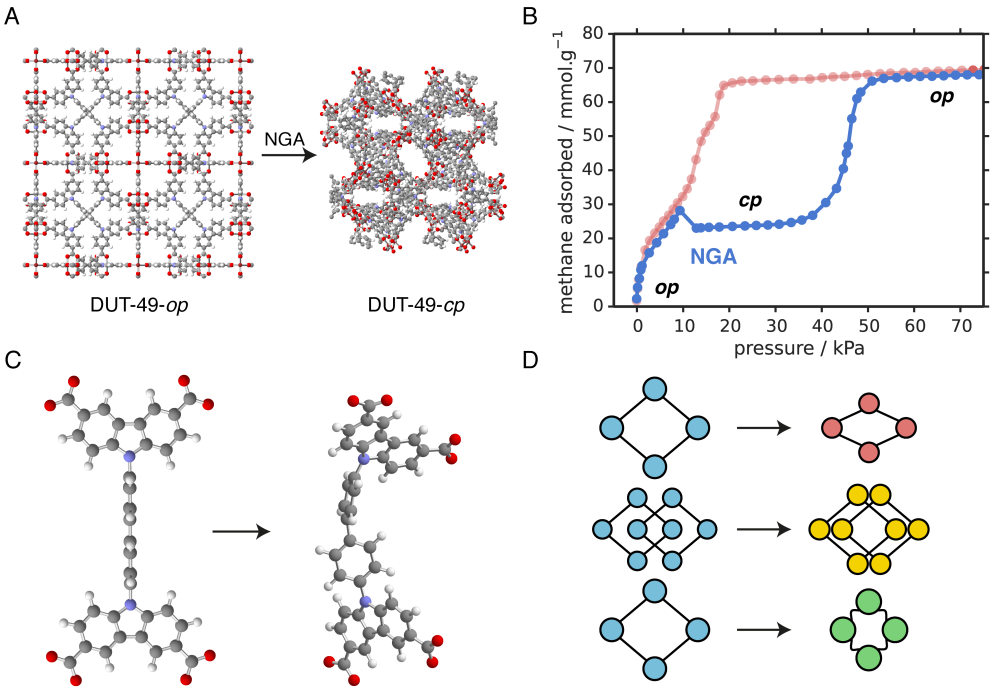

Figure 1: A summary of the crystal structure of DUT-49-*op* (open pore) and DUT-49-*cp* (contracted pore) including the transitions present during negative gas adsorption (NGA) and subsequent pore saturation (A). An example of the experimental isotherm observed for DUT-49 during methane adsorption at 111 K (B, blue) and the type 1 isotherm, calculated by simulation, for the static DUT-49-*op* structure (B, red).[8] Buckling-like deformation of the BBCDC ligand demonstrated during the NGA process (C). Stylistic representation of structural transformations in MOFs: hinging mechanism (red), sub-lattice displacement (yellow) and the mechanism observed in DUT-49 (green).

buckling is characterized by a sudden sideways failure of a structure subjected to significant axial compressive stress, where the compressive stress at the point of failure is less than the ultimate compressive stress that the material is capable of withstanding. To test the relevance of this analogy, we performed DFT optimizations of a single isolated ligand with a series of fixed decreasing N atom to N atom distance. All other internal coordinates were freely optimized. By derivating the energy–strain curve, we obtain a stress–strain profile depicted in Figure 2. Moreover, the constrained structures clearly reflect the dihedral like rotation of carbazole moieties when the linker is compressed and bends, as observed in the experimental contracted

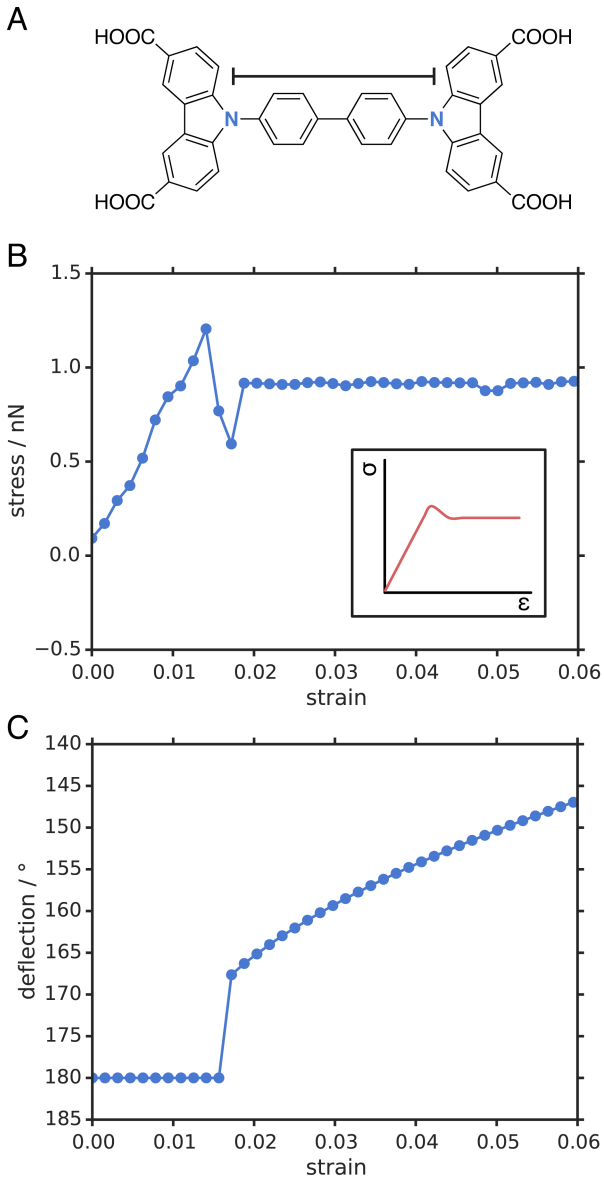

Figure 2: (A) BBCDC ligand with the N atom to N atom distance highlighted. (B) Stress–strain curve of the BBCDC ligand relative to axial compression; in inset, a typical stress-strain curves found for macroscopic materials with buckling.[17] (C) Deflection angle of the ligand, measured as N–centroid–N angle.

pore structure. We quantify the bending of the linker by a "deflection" parameter, which we take as the N–centroid–N angle.

Figure 2 reveals two distinct regimes upon the application of strain to the ligand. Firstly, small deformations result in no deflection as the ligand retains a linear structure. This elastic regime merely corresponds to the compression of interatomic bonds with, as expected, a linear response to deformation. For deformations greater than 3 Å a buckling transition occurs, with a sudden large deflection of the ligand and a non-linear mechanical response. Initially, by only considering the static structures of DUT-49-*op* and DUT-49-*cp* the energy cost of 91 kJ.mol^{-1} per ligand appears to be a significant penalty to the transformation. However, the analysis provided here shows the critical event requires significantly less energy at 10 kJ.mol^{-1}. Subsequently, upon the onset of buckling the ligand continues to collapse at constant stress.

The buckling of the ligand is in all features similar to that observed for macroscopic materials (represented as inset of Figure 2b). This elastic response of the ligand, which has not been previously observed in MOFs, produces a bending-dominated framework which is observed commonly with foam lattice-structured materials.[18] A consequence of the buckling feature in these materials is their stiffnesses are significantly reduced to that expected of stretch-dominated structures. For example, a typical foam with buckling behavior is less stiff by a factor of 10 than a stretch-dominated framework of the same density.[18] This mechanical perspective demonstrates how with modest stress the BBCDC ligand buckles thus producing an accessible pathway to a colossal change in volume of the DUT-49 structure.

Structural description and energetics

While DFT calculations show how the mechanical behavior of the organic ligand allow for the structural transition to take place, simulations are required at a larger scale to unveil the precise thermodynamics of NGA. Owing the large size of the DUT-49 unit cell, with 1 836 atoms, simulations at the DFT level have proved computationally prohibitive. We have thus used classical molecular dynamics simulation to capture the structure, energetics, and dynamics of the transition. The force field was based on the high-accuracy MOF-FF force field, which is known perform extremely well for MOFs and frameworks based on copper paddlewheels in particular. This was extended using MM3 for the organic parts (such as biphenyl unit) not available in MOF-FF.[19, 20]

To ensure the accuracy of the classical simulation methodology used here, we first generated trajectories of DUT-49-*op* and DUT-49-*cp* using initial configurations from DFT optimized structures. The 5 ns (N, P, T) simulations at 300 K and 1 atm demonstrate that the chosen potential parameters accurately describe the geometry and framework characteristics of both the open and contracted pore forms of the structure. We find that MOF-FF reproduces the unit cell parameters within $\approx 3\%$ of the experimental values for both the open and contracted pore structures. Additional details can be found in the Supporting Information. Notably, these differences are quite small considering that the force field was not adjusted on experimental data for DUT-49, and illustrates that the force field is applicable to both the open and contracted pore forms without scaling or further adjustment.

Furthermore, we computed a breakdown of the energy balance between the *op* and *cp* phases of DUT-49 in terms of various contributions to the average total energy, plotted in Figure 3: van der Waals (dispersion and repulsion) interactions, bond stretching, bending, torsion, and out-of-plane energies. This analysis, which can be performed due to the analytical nature of the interactions described by the force field, clearly illustrates the balance of intramolecular strain (dominated by torsion energy and favoring the *op* structure) and intermolecular dispersive interactions (favoring the *cp* structure) which results in a significantly smaller energy penalty to the distorted DUT-49-*cp* structure. Overall, we find that the *op* phase is energetically more stable than the *cp* phase (by 270 kJ.mol^{-1} per unit cell) in the absence of adsorbate, which is in line with experimental data.

Transition dynamics

We next turn to the description by molecular simulations of the actual transition between the two metastable structures *op* and *cp* of DUT-49. Experimentally, Kaskel and coworkers have shown that these structural transitions can be caused by adsorption and desorption of guest molecules.[8] Because the stable form of the evacuated material at ambient conditions is that with largest volume (*op*), it is expected from thermodynamics that the *op*→*cp* transition can also be triggered by application of external pressure — as is the case for the "breathing" transition in MIL-53 and MIL-47 materials.[12, 21]

In order to check this hypothesis and observe the transition dynamics in the simplest possible case, without adsorbate, we performed constant-pressure simulations where the pressure applied was varied over time. The

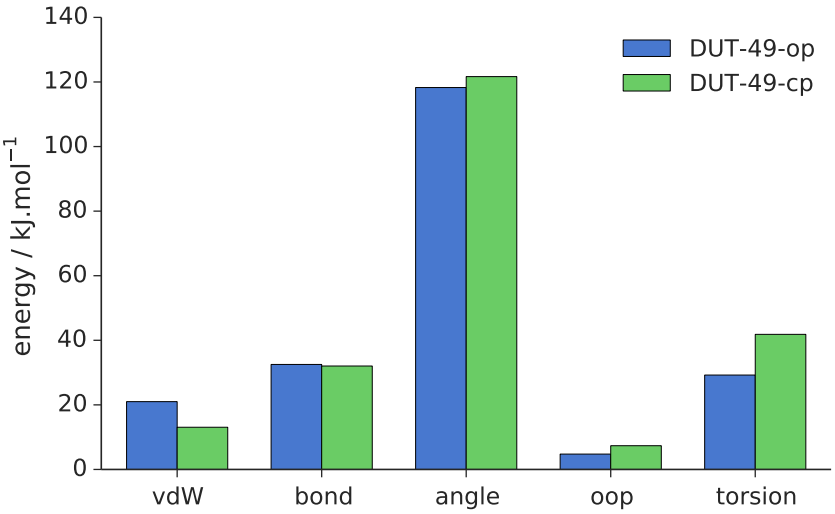

Figure 3: Average energy contributions, per ligand, for van der Waals (vdW), bond stretching, angle bending, out of plane (oop) and torsion terms during (N, P, T) simulations of guest-free DUT-49-*op* and DUT-49-*cp* at ambient conditions.

simulation trajectories, all conducted at 300 K, start from the *op* phase. They consist of 0.5 ns of initial equilibration at atmospheric pressure, a compression period with constant isotropic pressure $+P$ for 0.5 ns, additional equilibration at atmospheric pressure for 1 ns, a decompression (or tension) period with negative pressure $-P$ for 0.5 ns and a final equilibration at atmospheric pressure for 1 ns.

At modest pressure we only test the elastic behavior of the *op* structure upon compression and tension, with small variations in unit cell volume as can be seen on Figure 4a for $P = 50$ MPa (light blue curve). However, with pressure increments equal to or larger than $P = 60$ MPa, we see that the NGA transition is observed. The *op*→*cp* transition is observed upon compression the compression stage, confirming the possibility to trigger the NGA transition with a mechanical constraint. Upon release of the pressure, we find that the *cp* structure is retained, confirming its metastability in line with experimental findings. And finally, upon the application of equal opposite stress (negative pressure) the DUT-49-*op* structure is recovered.

To confirm the transformation is the result of the buckling of the BBCDC ligand, as described previously, the evolution of critical bond parameters were charted, displayed in the Supporting Information. We observe no significant

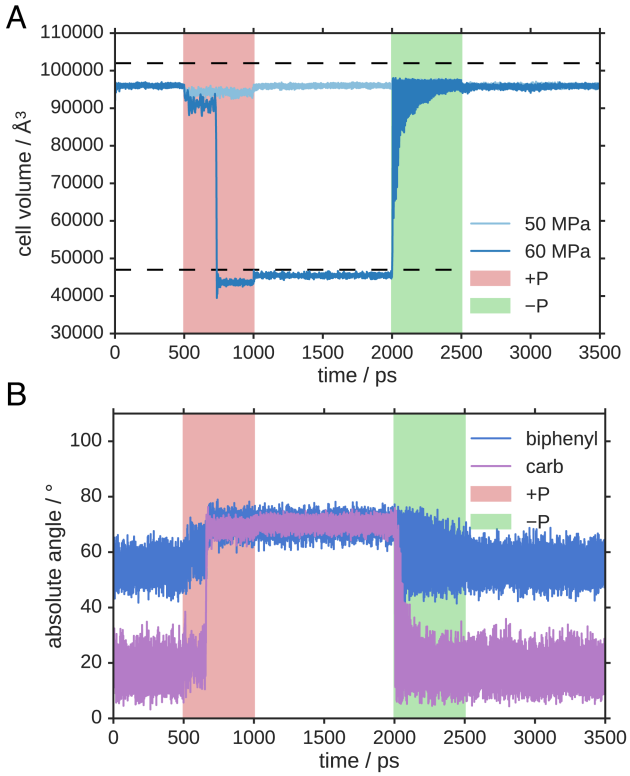

Figure 4: (A) Evolution of the unit cell volume during (N, P, T) simulations of DUT-49, with durations of applied pressure for a pressures of ± 50 and ± 60 MPa (see text for details). The volumes of *op* and *cp* phases at ambient conditions are indicated by dotted lines. (B) Averaged absolute dihedral angles of the biphenyl and carbazole (carb) moieties of the BBCDC ligand during these simulations.

changes in mean or standard deviation in bond lengths of Cu–Cu, Cu–O and C–N. However, we find significant and abrupt changes in N–N distances, biphenyl dihedrals and carbazole dihedrals during the trajectory, which are depicted in Figure 4b. These structural features are caused by buckling of the ligand, with the other features remaining invariable. Additionally, as found for the initial ambient condition simulations, the accounting of energy contributions during the trajectory explicitly illustrates the balance of energy between unfavorable torsional strain and favorable dispersion interactions.

Thermodynamics of negative gas adsorption

For solids with multiple phases and structural transitions, the analysis of their free energy as a function of volume, $F(V)$, yields crucial insight into the relative stability and metastability of the respective phases. This was, for example, recently applied to the case of adsorption in the "breathing" MOF MIL-53(Al).[22] In practice, the $F(V)$ curve can be calculated by thermodynamic integration of the internal pressure of the system as a function of volume. Several constant-volume (N, V, T) MD simulations are performed to obtain the internal pressure at each point, $P_i(V)$, in the range of volumes studied. Thus the free energy profile is derived as:

$$F(V) - F(V_{\text{ref}}) = -\int_{V_{\text{ref}}}^{V} \langle P_i(V') \rangle \, \mathrm{d}V' \tag{1}$$

where we chose as reference volume V_{ref} the open pore structure. The resulting profiles of internal pressure and free energy landscapes are plotted on Figure 5. In addition, the internal energy U was also calculated at each point.

The pressure profile of DUT-49 (Figure 5a) reveals the stable and metastable structures found at a given external pressure. Crystal structures of the two distinct phases of DUT-49 were measured at atmospheric pressure and according to the profile, three structures correspond to this pressure: the open pore form, the contracted pore form, and a transition state situated between these. However, the positive derivative $\left(\frac{\partial P}{\partial V}\right)$ observed at the transition state makes it mechanically unstable. Further analysis of this pressure landscape also predicts how the DUT-49 structure evolves when decreasing or increasing the external pressure as, at mechanical equilibrium, the internal pressure is equivalent to the external pressure. For pressures above ≈ 60 MPa, we find only one stable state exists where the system remains the contracted pore state. Contrastingly, DUT-49 exists as the large pore structure for pressures below ≈ -60 MPa. In between, the two phases are metastable, in line with both experimental data and the results of direct molecular dynamics under pressure.

Notably, the pressure required to achieve buckling ($\approx$ 60 MPa) is in the range of adsorption-induced stresses, exerted by adsorbed fluids on the solid.[23] Thus it is unsurprising that the transition *op*→*cp* is observed during gas adsorption experiments.

The free energy profile generated for DUT-49 (Fig. 5b) shows two distinct minima corresponding to the contracted and open pore structures. Additionally, there exists a energetic barrier of $\Delta F^{\ddagger} = 130$ kJ.mol^{-1} to the contracted to open pore transition which prohibits the contracted structure from spontaneously opening to the large pore structure without external stimuli. This mirrors experimental observations in which stress by gas adsorption at saturation is required to regenerate the open pore structure.[8] A free energy difference between the two phases of $\Delta F = 1\,010$ kJ.mol^{-1} is predicted (per unit cell). The magnitude of this difference is in good agreement to the $2\,184$ kJ.mol^{-1} energy difference reported previously using DFT methods, despite the two totally different approaches and level of theory.

Finally, the entropy of the DUT-49 structural transition can be established by comparing the free energy and internal energy profiles obtained from the classical molecular simulation, demonstrated in Figure 5b, as $F = U - TS$. Remarkably, we find that the role of entropy is small in the transition, which is mainly driven by energetic contributions. The entropy difference between the *op* and *cp* phases is calculated to be $\Delta S = 0.0433$ kJ.mol^{-1}.K^{-1}, and entropy plays a larger role in the free energy barrier to the transition ($\Delta S^{\ddagger} = 0.184$ kJ.mol^{-1}.K^{-1}). This is in stark contrast with the structural transitions previously observed in "breathing" MOFs, where the flexibility is based on a hinging mechanism and deformation of coordination at the metal center. In those materials, which have been extensively studied from the thermodynamic point of view, the transition is known to be linked to a balance between energetic and entropic criteria.[24, 25] Thus, one outcome is that temperature has little effect on the relative energies of the phases of DUT-49, and the transition cannot be triggered by changes in temperature, unlike in MIL-53 materials.

Transition upon gas adsorption

After demonstrating that the structural transition in DUT-49 can be triggered by mechanical pressure in a guest-free framework, and given insight into its thermodynamics, we now turn to understanding the thermodynamics of adsorption for the novel phenomenon of negative gas adsorption. By combining free energy simulations, as described previously, with increasing amount of methane present in the simulation cell we are able to chart the stability of the two phases at various points over the entire isotherm. (N, V, T) simulations were this time performed at 120 K, comparable to the conditions observed for NGA, with methane loadings of 200, 400, 600, 800 and 1000

molecules per unit cell. Subsequently, these simulations result in valuable thermodynamic information, including variation of the free energy profiles as illustrated in Figure 6.

Table 1: Differences in total energy (U, kJ.mol^{-1}), free energy (F, kJ.mol^{-1}) and entropy (S, kJ.K^{-1}mol^{-1}) for the transition DUT-49-*op*→DUT-49-*cp*, calculated from NVT simulations at 120 K with increasing amount of methane molecules (molecules per unit cell).

CH_4 adsorbed	ΔU	ΔF	ΔS
0	1 020	1 010	0.0833
200	68.6	234	−1.38
400	−979	−57.1	−7.68
600	−155	1 380	−12.8
800	2 390	8 360	−49.8
1 000	17 100	26 000	−74.2

Upon methane adsorption, DUT-49 begins in the *op* phase as this corresponds to most energetically favorable phase. However, as the methane loading increases up to 400 molecules per unit cell (20.2 mmol.g^{-1}), the *cp* phase is stabilized and becomes the most thermodynamically favorable phase. This is due to the host–guest interactions being more favorable in the contracted structure, due to smaller wall–wall distances, and the low entropic cost corresponding to this loading of methane (Table 1). Despite this shift in global minima there remains a significant barrier, of the order of 300 kJ.mol^{-1}, associated with the *op*→*cp* transition. Upon further methane adsorption to 600 molecules per unit cell (30.4 mmol.g^{-1}) the barrier to transition decreases to ≈ 180 kJ.mol^{-1} allowing the structure to explore higher density phases. Importantly, we find the free energy landscape for this loading does not include a minima at the *cp* phase as there is significant entropic expense to condensing the quantity of methane in a low capacity pore structure. We thus conclude that by undergoing NGA, releasing methane from the structure, the structure can transform from a metastable state, at 600 molecules per unit cell to a stable *cp* phase, at 400 molecules per unit cell.

Finally, as the amount of methane increases to saturation the low capacity *cp* state is unfavorable due to guest–guest and guest–wall short-range repulsion; the stable structure at these loadings is then the highly porous *op* phase, accounting for the "reopening" *cp*→*op* transition. This thermodynamic analysis, presented here, allows us to provide a precise understanding of the structural transformations during gas adsorption. In addition, we

demonstrate an interplay between the driving forces of the framework and the adsorption process, which gives rise to NGA.

Conclusion

We have used a multiscale computational approach to shed light into the energetics, dynamics and thermodynamics of the negative gas adsorption phenomenon in highly flexible MOF DUT-49. By using DFT simulations we find that the complex yet compliant structure of the DUT-49 ligand allows for its buckling upon modest stress. The elastic coupling of these buckling units allows for the large-scale structural transformation of the entire framework, which is thus significantly softer than would be expected for rigid building units. This microscopic mechanism for flexibility is entirely new and presents a great contrast with previously known flexible MOFs, which relied either on sub-lattice displacement or hinging around metal nodes — with rigid linkers.

Furthermore, we have investigated the NGA transition using molecular dynamics simulations. We demonstrated that NGA requires a bistable porous material where the empty open pore (*op*) phase is thermodynamically more stable, but the contracted pore (*cp*) phase is metastable at ambient conditions. In addition to this generic criteria, which many "breathing" MOFs may exhibit, negative gas adsorption, requires the relative stability of *cp* and *op* phases to change with gas adsorption. Specifically, we expect the decreased transition barrier, observed for DUT-49 at 600 molecules per cell of methane, accompanying the absence of a minima at the *cp* volume to be a crucial feature of this process. We also showed that the structural transition in DUT-49 can be triggered by purely mechanical constraints, in the absence of guest molecules.

The insight provided by this investigation has elucidated the mechanics and thermodynamics that govern the phenomenon of negative gas adsorption, and will undoubtedly aid in the discovery of other systems with this desirable property.

Simulation Methods

The behavior and mechanical properties of the BBCDC ligand were investigated, for the corresponding acid, using DFT optimizations employed by the CRYSTAL14 software[26] with localized TZVP basis sets[27] and the

hybrid exchange–correlation functional PBE0.[28] Long-range dispersion corrections were included by using the Grimme "D2" approach.[29] The ligand structure was strained by decreasing the N atom to N atom length from the local minima at 9.827 Åto 9.227 Å, in 40 steps. At each step the structures were optimized with the N atom to N atom length held fixed. Consequently, a stress-strain curve relative to this axial deformation of the ligand was generated, where stress is defined by the gradient of energy and strain the relative decrease in N atom to N atom length.

Initial periodic structures of DUT-49-*op* and DUT-49-*cp*, which correspond respectively to the open pore (*op*) and contracted pore (*cp*) structures, were obtained from DFT optimized models reported by Krause *et al.*[8] Classical simulations used the MOF-FF forcefield to describe the unsaturated Cu paddlewheels present in the structure.[30] Parameters missing from MOF-FF, for the description of the ligand and methane, were taken from the MM3 forcefield for organic molecules, which is itself the basis of MOF-FF.[19, 20] Importantly, we have treated the dihedral parameters of the ligand as to allow unrestricted rotation of the phenyl groups that make up the biphenyl section. Classical molecular dynamics simulations were undertaken using the `pydlpoly` software by Schmidt and coworkers,[31] a Python-wrapped version of DL_POLY Classic.[32] To first ensure the accuracy of the force field and potential parameters chosen, (N, P, T) simulations were completed for DUT-49-*op* and DUT-49-*cp*. We then studied the NGA transition by performing series of (N, V, T) simulations at varying guest loading N and volume V. Constant-volume simulations were used to compute the average internal pressure for a given volume, with an initial 100 ps for equilibration and the final 500 ps sampled to obtain a converged value of internal pressure.[1] From a series of constant-volume simulations we could thus integrate the internal pressure to find free energy profiles as a function of volume.[22] This was repeated with the addition of increasing number of methane molecules to the simulation cell, which were grown in during initial equilibration. All classical molecular dynamics simulations used a time step of 1 fs and employed the Nosé-Hoover thermostat and barostat,[33, 34] for the (N, P, T) simulations, with a thermostat relaxation time of 1 ps and barostat relaxation time of

[1] We note previous work on the mechanical characterization of MIL-47(Al), the $(N, V, \sigma_a = 0, T)$ ensemble was used which allows for the cell shape to change during the simulation.[22] However, as this transition does not involve a change in cell shape (cubic to cubic transition) the use of (N, V, T) simulation is appropriate.

2 ps.

Acknowledgements

The authors acknowledge PSL Research University for funding (project DEFORM, grant ANR-10-IDEX-0001-02) and HPC platforms provided by a GENCI grant (x2016087069). We also thank Dr Rochus Schmid for providing `pydlpoly`, and Simon Krause and Professor Stefan Kaskel for discussions and their continued collaboration.

References

[1] H. Furukawa, K. E. Cordova, M. O'Keeffe, O. M. Yaghi, The chemistry and applications of metal-organic frameworks, Science 341 (2013) 1230444–1230444.

[2] S. Horike, S. Shimomura, S. Kitagawa, Soft porous crystals, Nature Chemistry 1 (2009) 695–704.

[3] F.-X. Coudert, Responsive metal–organic frameworks and framework materials: Under pressure, taking the heat, in the spotlight, with friends, Chemistry of Materials 27 (2015) 1905–1916.

[4] S. Kitagawa, R. Kitaura, S. ichiro Noro, Functional porous coordination polymers, Angewandte Chemie International Edition 43 (2004) 2334–2375.

[5] J.-R. Li, Y. Ma, M. C. McCarthy, J. Sculley, J. Yu, H.-K. Jeong, P. B. Balbuena, H.-C. Zhou, Carbon dioxide capture-related gas adsorption and separation in metal-organic frameworks, Coordination Chemistry Reviews 255 (2011) 1791–1823.

[6] J. A. Mason, J. Oktawiec, M. K. Taylor, M. R. Hudson, J. Rodriguez, J. E. Bachman, M. I. Gonzalez, A. Cervellino, A. Guagliardi, C. M. Brown, P. L. Llewellyn, N. Masciocchi, J. R. Long, Methane storage in flexible metal–organic frameworks with intrinsic thermal management, Nature 527 (2015) 357–361.

[7] G. Férey, C. Serre, Large breathing effects in three-dimensional porous hybrid matter: facts, analyses, rules and consequences, Chemical Society Reviews 38 (2009) 1380.

[8] S. Krause, V. Bon, I. Senkovska, U. Stoeck, D. Wallacher, D. M. Többens, S. Zander, R. S. Pillai, G. Maurin, F.-X. Coudert, S. Kaskel, A pressure-amplifying framework material with negative gas adsorption transitions, Nature 532 (2016) 348–352.

[9] U. Stoeck, S. Krause, V. Bon, I. Senkovska, S. Kaskel, A highly porous metal–organic framework, constructed from a cuboctahedral super-molecular building block, with exceptionally high methane uptake, Chemical Communications 48 (2012) 10841.

[10] J. Rouquerol, F. Rouquerol, P. Llewellyn, G. Maurin, K. Sing, Adsorption by Powders and Porous Solids: Principles, Methodology and Applications, Elsevier Science, 2013.

[11] I. Beurroies, M. Boulhout, P. L. Llewellyn, B. Kuchta, G. Férey, C. Serre, R. Denoyel, Using pressure to provoke the structural transition of metal-organic frameworks, Angewandte Chemie International Edition 49 (2010) 7526–7529.

[12] A. V. Neimark, F.-X. Coudert, C. Triguero, A. Boutin, A. H. Fuchs, I. Beurroies, R. Denoyel, Structural transitions in MIL-53 (cr): View from outside and inside, Langmuir 27 (2011) 4734–4741.

[13] P. Serra-Crespo, A. Dikhtiarenko, E. Stavitski, J. Juan-Alcañiz, F. Kapteijn, F.-X. Coudert, J. Gascon, Experimental evidence of negative linear compressibility in the MIL-53 metal–organic framework family, CrystEngComm 17 (2015) 276–280.

[14] B. Chen, C. Liang, J. Yang, D. S. Contreras, Y. L. Clancy, E. B. Lobkovsky, O. M. Yaghi, S. Dai, A microporous metal–organic framework for gas-chromatographic separation of alkanes, Angewandte Chemie International Edition 45 (2006) 1390–1393.

[15] M. Schenk, S. D. Guest, Geometry of miura-folded metamaterials, Proceedings of the National Academy of Sciences 110 (2013) 3276–3281.

[16] J. L. Silverberg, A. A. Evans, L. McLeod, R. C. Hayward, T. Hull, C. D. Santangelo, I. Cohen, Using origami design principles to fold reprogrammable mechanical metamaterials, Science 345 (2014) 647–650.

[17] J. G. Eisley, A. M. Waas, Analysis of Structures, Wiley-Blackwell, 2011.

[18] M. Ashby, The properties of foams and lattices, Philosophical Transactions of the Royal Society A: Mathematical, Physical and Engineering Sciences 364 (2006) 15–30.

[19] N. L. Allinger, Y. H. Yuh, J. H. Lii, Molecular mechanics. the MM3 force field for hydrocarbons. 1, J. Am. Chem. Soc. 111 (1989) 8551–8566.

[20] J. H. Lii, N. L. Allinger, Molecular mechanics. the MM3 force field for hydrocarbons. 3. the van der waals potentials and crystal data for aliphatic and aromatic hydrocarbons, J. Am. Chem. Soc. 111 (1989) 8576–8582.

[21] P. G. Yot, Q. Ma, J. Haines, Q. Yang, A. Ghoufi, T. Devic, C. Serre, V. Dmitriev, G. Férey, C. Zhong, G. Maurin, Large breathing of the MOF MIL-47(VIV) under mechanical pressure: a joint experimental–modelling exploration, Chemical Science 3 (2012) 1100.

[22] S. Rogge, L. Vanduyfhuys, A. Ghysels, M. Waroquier, T. Verstraelen, G. Maurin, V. V. Speybroeck, A comparison of barostats for the mechanical characterization of metal–organic frameworks, J. Chem. Theory Comput. 11 (2015) 5583–5597.

[23] P. I. Ravikovitch, A. V. Neimark, Density functional theory model of adsorption deformation, Langmuir 22 (2006) 10864–10868.

[24] A. Boutin, M.-A. Springuel-Huet, A. Nossov, A. Gédéon, T. Loiseau, C. Volkringer, G. Férey, F.-X. Coudert, A. H. Fuchs, Breathing transitions in MIL-53(al) metal-organic framework upon xenon adsorption, Angewandte Chemie International Edition 48 (2009) 8314–8317.

[25] F.-X. Coudert, A. U. Ortiz, V. Haigis, D. Bousquet, A. H. Fuchs, A. Ballandras, G. Weber, I. Bezverkhyy, N. Geoffroy, J.-P. Bellat, G. Ortiz, G. Chaplais, J. Patarin, A. Boutin, Water adsorption in flexible gallium-based MIL-53 metal–organic framework, J. Phys. Chem. C 118 (2014) 5397–5405.

[26] R. Dovesi, R. Orlando, A. Erba, C. M. Zicovich-Wilson, B. Civalleri, S. Casassa, L. Maschio, M. Ferrabone, M. D. L. Pierre, P. D'Arco, Y. Noël, M. Causà, M. Rérat, B. Kirtman, C RYSTAL14 : A program for the ab initio investigation of crystalline solids, Int. J. Quantum Chem. 114 (2014) 1287–1317.

[27] M. F. Peintinger, D. V. Oliveira, T. Bredow, Consistent gaussian basis sets of triple-zeta valence with polarization quality for solid-state calculations, J. Comput. Chem. 34 (2012) 451–459.

[28] C. Adamo, V. Barone, Toward reliable density functional methods without adjustable parameters: The PBE0 model, The Journal of Chemical Physics 110 (1999) 6158.

[29] S. Grimme, Semiempirical GGA-type density functional constructed with a long-range dispersion correction, J. Comput. Chem. 27 (2006) 1787–1799.

[30] S. Bureekaew, S. Amirjalayer, M. Tafipolsky, C. Spickermann, T. K. Roy, R. Schmid, MOF-FF - a flexible first-principles derived force field for metal-organic frameworks, Phys. Status Solidi B 250 (2013) 1128–1141.

[31] S. Bureekaew, R. Schmid, Hypothetical 3d-periodic covalent organic frameworks: exploring the possibilities by a first principles derived force field, CrystEngComm 15 (2013) 1551.

[32] W. Smith, T. Forester, DL_POLY_2.0: A general-purpose parallel molecular dynamics simulation package, Journal of Molecular Graphics 14 (1996) 136–141.

[33] W. G. Hoover, Canonical dynamics: Equilibrium phase-space distributions, Phys. Rev. A 31 (1985) 1695–1697.

[34] S. Melchionna, G. Ciccotti, B. L. Holian, Hoover NPT dynamics for systems varying in shape and size, Molecular Physics 78 (1993) 533–544.

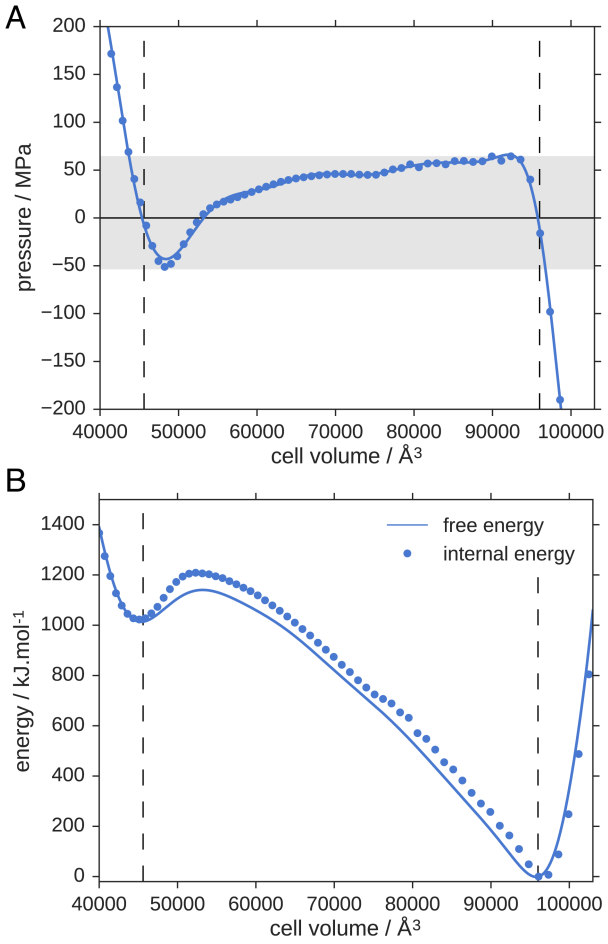

Figure 5: Internal pressure (A) and energy (B) profiles as a function of unit cell volume, obtained from (N, V, T) simulations at 300 K. The pressure from simulation is displayed as points with the polynomial fit as a line. Furthermore, we highlight in gray the pressure range for which the structure can exist as two different metastable states. Internal energy is displayed in panel (B) as points compared to free energy, calculated by thermodynamic integration, depicted as a line. Additionally, we feature the volume of *op* and *cp* phases as dotted lines.

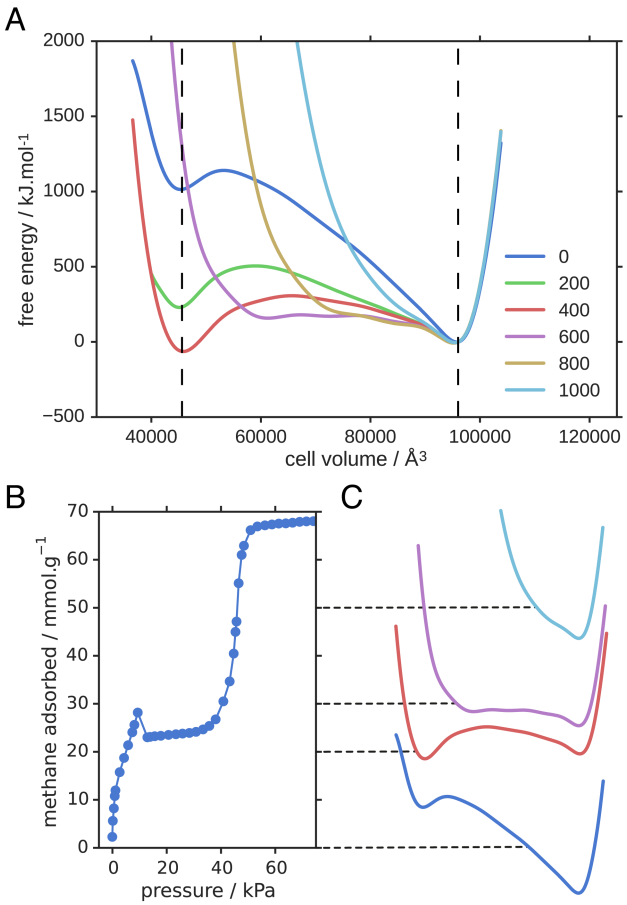

Figure 6: Free energy profiles as a function of unit cell volume (A), obtained from NVT simulations at 120 K with increasing amount of methane molecules (molecules per unit cell) and volumes corresponding to the *op* and *cp* phases are displayed as dotted lines. The methane isotherm for DUT-49 at 111 K (B) shown with corresponding free energy profile for a given methane loading (C).

Supporting information for:

Origins of Negative Gas Adsorption

Jack D. Evans,[†] Lydéric Bocquet,[‡] and François-Xavier Coudert[*,†]

[†]*Chimie ParisTech, PSL Research University, CNRS, Institut de Recherche de Chimie Paris, 75005 Paris, France*

[‡]*Laboratoire de Physique Statistique, École Normale Supérieure, UMR CNRS 8550, PSL Research University, 24 rue Lhomond, 75005 Paris, France*

E-mail: fx.coudert@chimie-paristech.fr

Table S1: Average cell parameters of DUT-49 obtained from a 5 ns (N,P,T) molecular dynamics simulations simulations at 300 K and 1 atm. Parameters found using DFT are displaying in italics.

	DUT-49-*op*	DUT-49-*cp*
volume / Å^3	96000 $\pm$ 300 *(102000)*	45600 $\pm$ 400 *(47300)*
a / Å	45.8 $\pm$ 0.1 *(46.72)*	35.7 $\pm$ 0.4 *(36.18)*
b / Å	45.8 $\pm$ 0.1 *(46.72)*	35.7 $\pm$ 0.4 *(36.18)*
c / Å	45.8 $\pm$ 0.1 *(46.72)*	35.7 $\pm$ 0.4 *(36.18)*
α / $^\circ$	90.0 $\pm$ 0.5 *(90.0)*	90.0 $\pm$ 0.7 *(90.0)*
β / $^\circ$	90.0 $\pm$ 0.5 *(90.0)*	90.0 $\pm$ 0.7 *(90.0)*
γ / $^\circ$	90.0 $\pm$ 0.5 *(90.0)*	90.0 $\pm$ 0.6 *(90.0)*

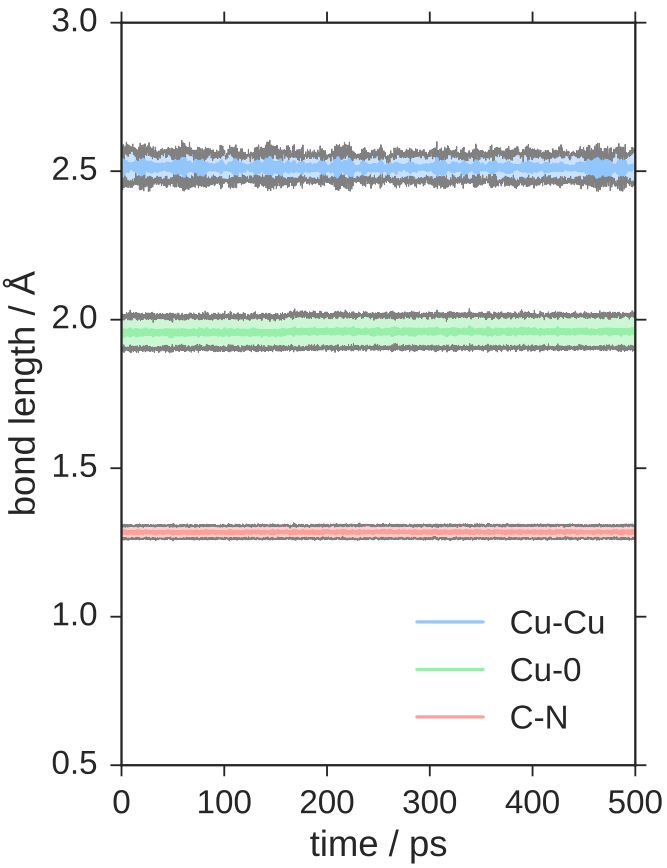

Figure S1: Mean and standard deviation (depicted by a lighter color) of critical bond lengths during the compression period of (N,P,T) simulations with constant isotropic pressure of 60 MPa for 0.5 ns.

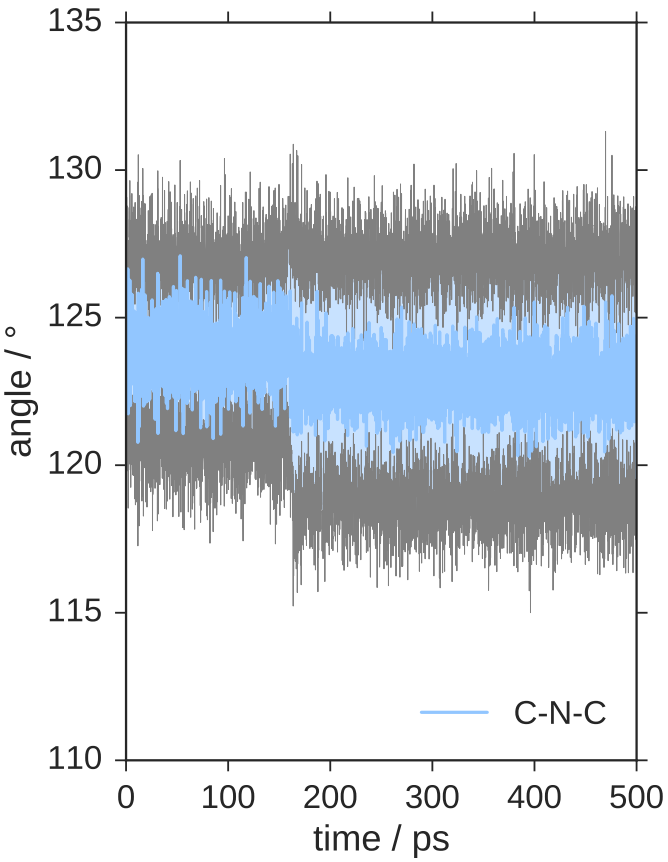

Figure S2: Mean and standard deviation (depicted by a lighter color) of carbazole angles during the compression period of (N,P,T) simulations with constant isotropic pressure of 60 MPa for 0.5 ns.

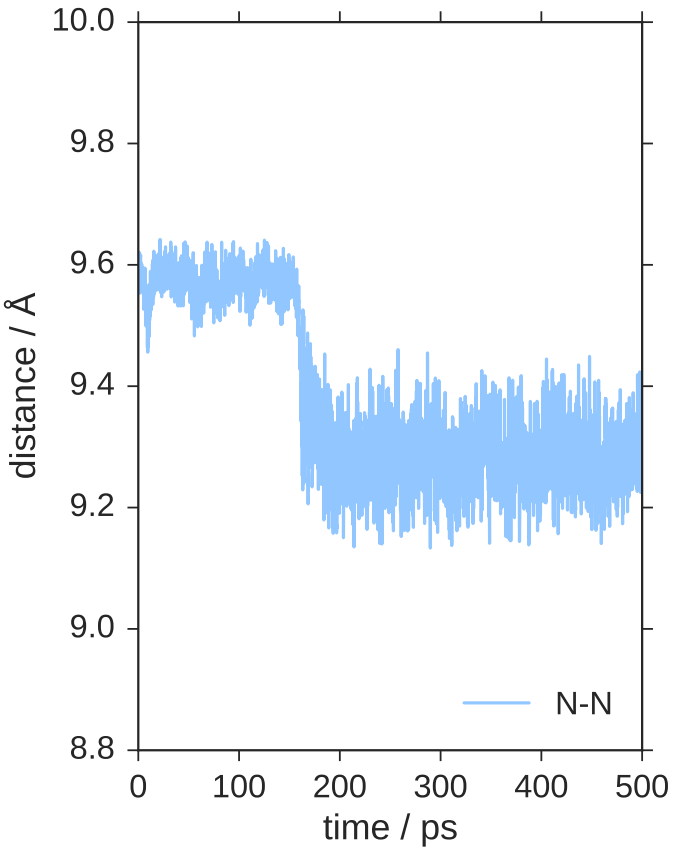

Figure S3: Mean and standard deviation (depicted by a lighter color) of ligand N–N distance during the compression period of (N,P,T) simulations with constant isotropic pressure of 60 MPa for 0.5 ns.

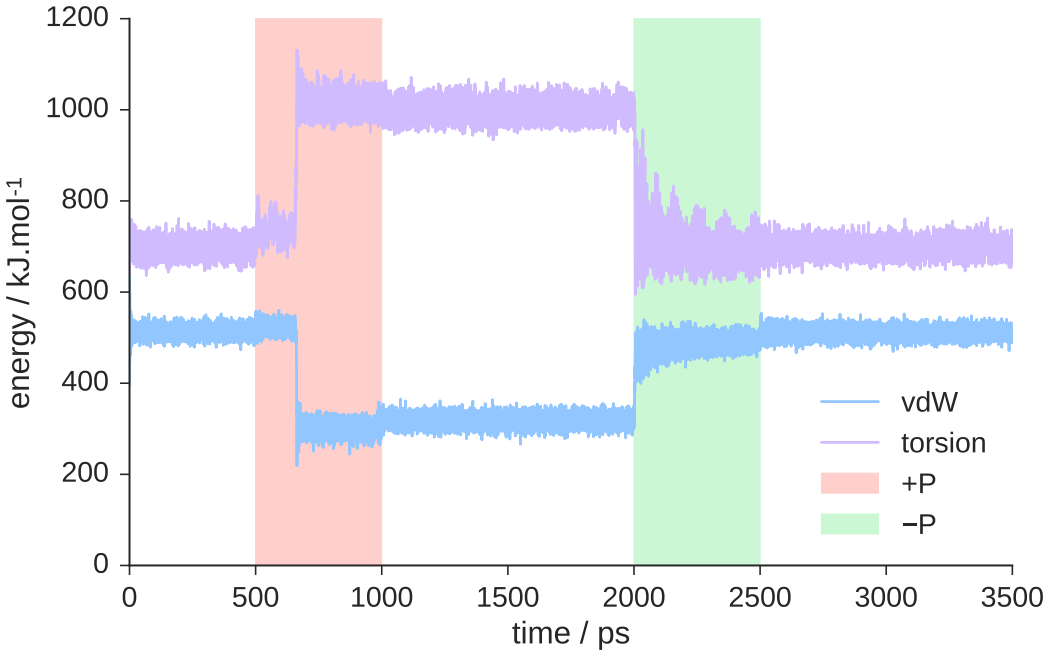

Figure S4: Energy contributions for van der Waals (vdW) and torsion terms during *NPT* simulations with durations of applied pressure for a pressure of $\pm$60 MPa.

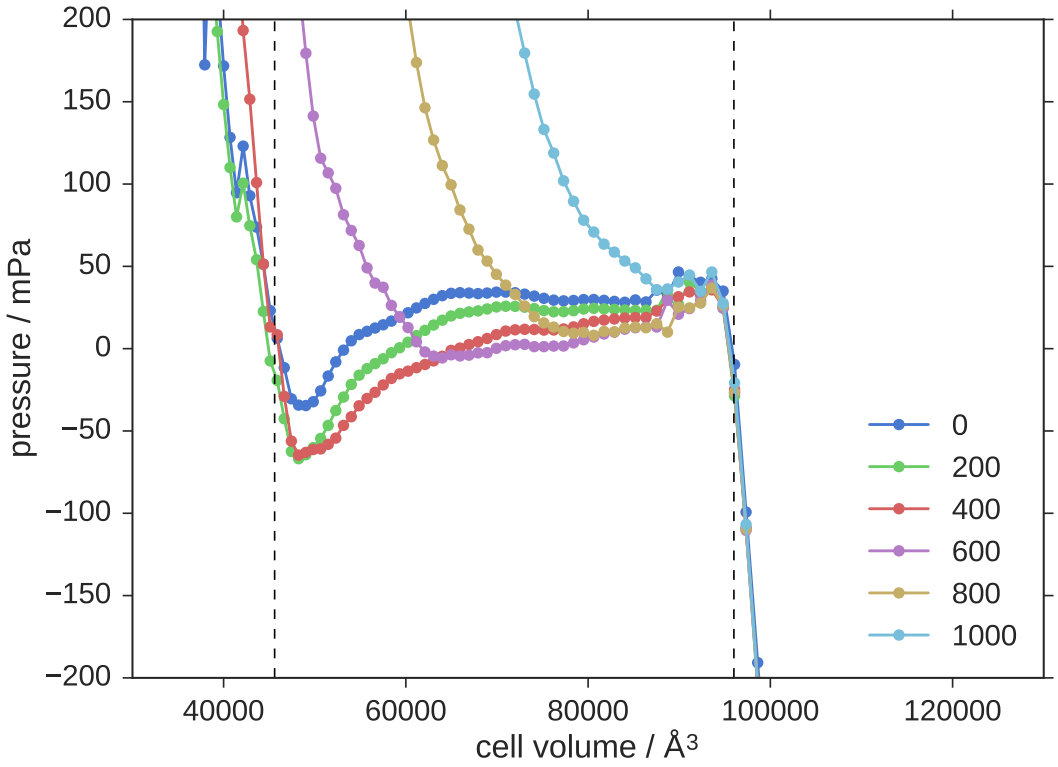

Figure S5: Internal pressure profiles as a function of unit cell volume, obtained from (N,V,T) simulations at 120 K with increasing amount of methane molecules (molecules per unit cell).

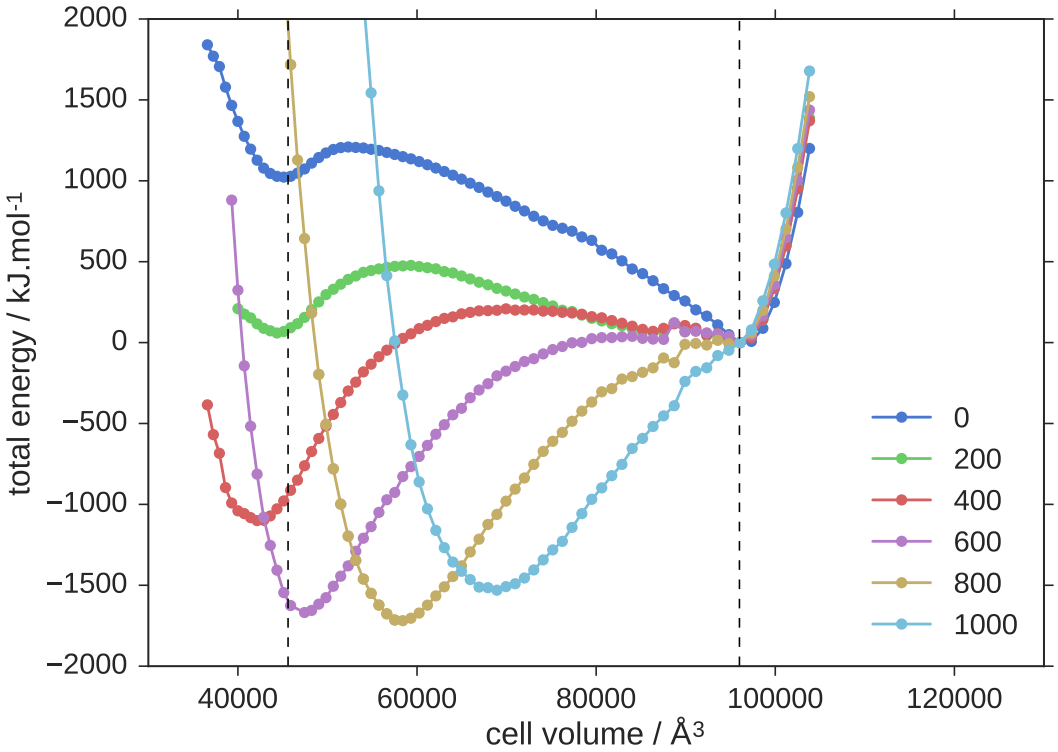

Figure S6: Total energy profiles as a function of unit cell volume, obtained from (N,V,T) simulations at 120 K with increasing amount of methane molecules (molecules per unit cell).